Central WENO schemes through a global average weight

Antonio Baeza · Raimund Bürger ·
Pep Mulet · David Zorío

November 22, 2017

Abstract A novel central weighted essentially non-oscillatory (central WENO; CWENO)-type scheme for the construction of high-resolution approximations to discontinuous solutions to hyperbolic systems of conservation laws is presented. This procedure is based on the construction of a global average weight using the whole set of Jiang-Shu smoothness indicators associated to stencil. By this device one does not to have to rely on ideal weights, which, under certain stencil arrangements and interpolating point locations, do not define a convex combination of the interpolating lower-degree polynomials of the corresponding sub-stencils. Moreover, this procedure also prevents accuracy loss near smooth extrema. These properties result in a more flexible scheme that overcomes these issues, at the cost of only few additional computations with respect to classical WENO schemes. Numerical examples illustrate the performance of the new CWENO schemes.

———————————————

A. Baeza · P. Mulet
Departament de Matemàtiques
Universitat de València
E-46100 Burjassot, Spain
E-mail: antonio.baeza@uv.es, mulet@uv.es

R. Bürger
CI^{2}MA & Departamento de Ingeniería Matemática
Universidad de Concepción
Casilla 160-C, Concepción, Chile
E-mail: rburger@ing-mat.udec.cl

D. Zorío
CI^{2}MA, Universidad de Concepción
Casilla 160-C, Concepción, Chile
E-mail: dzorio@ci2ma.udec.cl

1 Introduction

1.1 Scope

Weighted Essentially Non-Oscillatory (WENO) schemes [7,9] have been widely used in the literature, especially in the context of the approximation of discontinuous solutions to hyperbolic systems of conservation laws. The main feature of the WENO procedure is based on the fact that a reconstruction polynomial can be decomposed as a certain convex combination of reconstruction polynomials of lower order, provided they are evaluated at points within a certain range. This property is attained in the case of the well-known classical odd-order WENO schemes, both when the WENO procedure is applied for interpolation of a function from point values (as is expounded in [12, Sect. 2.1]) and for the reconstruction of a function from cell averages (see [12, Sect. 2.2]). The latter usage is more relevant to the numerical solution of conservation laws. The weights used to ponder the contribution of each lower-order polynomial depend on the interpolating point and are known as ideal weights. WENO schemes define nonlinear weights based on the ideal weights so as to construct an essentially non oscillatory interpolant. However, there are some circumstances in which the ideal linear weights are negative and thus the non-linear WENO weights do not satisfy the required properties, namely to attain the optimal order under smoothness assumptions and to be essentially non-oscillatory when a discontinuity crosses the stencil. This is a well-known problem and strategies to solve it are summarized in [12, Sect. 2.3.3]. Therefore, since there are some practical situations in which classical WENO schemes are not suitable for use, some authors have proposed solutions to overcome the aforementioned issues by introducing the so-called central WENO (CWENO) schemes [8].

It is the purpose of this paper to propose an alternative approach to the previous works, based on a global average weight which does not depend on the ideal weights and is built using only the classical Jiang-Shu smoothness indicators [7] that would be considered to compute the classical WENO weights. Hence, it suffices to consider only two additional items: on one hand, the global average weight, which is defined using the smoothness indicators through elementary operations; and on the other hand, the evaluation of the reconstruction polynomial from the whole stencil. Therefore, it is expected that the computational cost regarding this scheme is not much higher than for classical WENO schemes.

Finally, it should be remarked as well that, as will be shown along the paper, this procedure is also capable to overcome the issue of loss of order of accuracy near smooth extrema associated with the original WENO schemes.

1.2 Related work

To further put the paper into the proper perspective, we recall that WENO schemes build on the previously family of essentially nonoscillatory (ENO) schemes that are based on selecting the least oscillatory polynomial for reconstruction (among several available candidates defined by their respective stencils), see Harten et al. [5] and Shu and Osher [13,14]. The underlying idea of WENO schemes, namely to utilize a weighted combination of these polynomials, was introduced in [9] and put into a general framework to construct arbitrary-order accurate finite

difference schemes in [7]. These schemes have gained a vast amount of popularity and interest. For general information and references also to applications we refer to review articles and handbook entries including [11, 12, 15].

The concept of central WENO (CWENO) schemes was advanced first by Levy, Doron and Russo [8], where a new reconstruction polynomial, based on the information of the whole stencil, together with the addition of an ideal weight associated to such reconstruction, is proposed. This modification allows to attain the optimal order for any convex combination of such weights, yielding a much more versatile scheme. See also [3] and references therein for further details regarding the aforementioned schemes.

1.3 Outline of the paper

The remainder of the paper is divided as follows. In Section 2, we briefly present the context in which we will stress out the performance of the proposed scheme along the paper. Section 3 is devoted to the description of the novel CWENO scheme in full detail. A motivation for developing such technique is presented in Section 3.1, in which some cases are shown in which classical WENO schemes fail to provide a satisfactory strategy to perform spatial reconstructions. Section 3.2 is focused on the formulation of our new scheme. Finally, in Section 3.3 some theoretical results involving the accuracy of the weights and the reconstructions through our scheme are shown. Next, in Section 4, several numerical tests are presented in order to validate with numerical evidence the theoretical considerations drawn in the previous sections regarding the scheme presented in this paper. On one hand, Section 4.1 is devoted to an extensive accuracy analysis; on the other hand, Section 4.2 is focused on several tests to check the behaviour of the proposed scheme in shock problems from hyperbolic conservation laws, and to compare them with the results obtained through the classical WENO scheme.

Finally, in Section 5 some conclusions are drawn.

2 Equations and numerical method

Although WENO schemes are an approximation not directly related to numerical schemes for a determined type of PDE, we focus on hyperbolic conservation laws. Therefore, we will briefly describe in this section the equations and their discretization procedure. The partial differential equations (PDEs) considered in this work are hyperbolic systems of m scalar conservation laws in d space dimensions:

$$\boldsymbol{u}_t + \sum_{i=1}^{d} \boldsymbol{f}^i(\boldsymbol{u})_{x_i} = \boldsymbol{0}, \quad (\boldsymbol{x}, t) \in \Omega \times \mathbb{R}^+ \subseteq \mathbb{R}^d \times \mathbb{R}^+, \quad \boldsymbol{x} = (x_1, \ldots, x_d), \quad (2.1)$$

where $\boldsymbol{u} = \boldsymbol{u}(\boldsymbol{x}, t) \in \mathbb{R}^m$ is the sought solution, $\boldsymbol{f}^i : \mathbb{R}^m \to \mathbb{R}^m$ are given flux density vectors, and

$$\boldsymbol{u} = \begin{pmatrix} u_1 \\ \vdots \\ u_m \end{pmatrix}, \quad \boldsymbol{f}^i = \begin{pmatrix} f_1^i \\ \vdots \\ f_m^i \end{pmatrix}, \quad i = 1, \ldots, d, \quad \boldsymbol{f} = \begin{bmatrix} f^1 \ldots f^d \end{bmatrix}.$$

System (2.1) is complemented with the initial condition

$$u(\boldsymbol{x}, 0) = \boldsymbol{u}_0(\boldsymbol{x}), \quad \boldsymbol{x} \in \Omega,$$

and prescribed boundary conditions.

To describe the spatial discretization, we introduce a Cartesian grid $\mathcal{G}$ formed by points (cell centers) $\boldsymbol{x} = \boldsymbol{x}_{j_1,\dots,j_d} = ((j_1 - \frac{1}{2})h, \dots, (j_d - \frac{1}{2})h) \in \mathcal{G}$ for $h > 0$. In what follows, we use the index vector $\boldsymbol{j} = (j_1, \dots, j_d)$, let $\boldsymbol{e}_i$ denote the i-th d-dimensional unit vector, and assume that J is the set of all indices $\boldsymbol{j}$ for which point values need to be updated. We then define

$$\boldsymbol{U}(t) := \big(\boldsymbol{u}(\boldsymbol{x}_{\boldsymbol{j}}, t)\big)_{\boldsymbol{j} \in J}.$$

Then we utilize the Shu-Osher finite difference scheme [14] with upwind spatial reconstructions of the flux function that are incorporated into numerical flux vectors $\hat{\boldsymbol{f}}^i$ through a Donat-Marquina flux-splitting [4]. Thus, the contribution to the flux divergence in direction x_i at point $\boldsymbol{x} = \boldsymbol{x}_{\boldsymbol{j}}$ is given by

$$\boldsymbol{f}^i(\boldsymbol{U})_{x_i}(\boldsymbol{x}_{\boldsymbol{j}}, t) \approx \frac{1}{h}\Big(\hat{\boldsymbol{f}}^i_{\boldsymbol{j}+\frac{1}{2}\boldsymbol{e}_i}\big(\boldsymbol{U}(t)\big) - \hat{\boldsymbol{f}}^i_{\boldsymbol{j}-\frac{1}{2}\boldsymbol{e}_i}\big(\boldsymbol{U}(t)\big)\Big).$$

As a particular case of interest we consider WENO reconstructions [7] of order $2r+1$. To specify the time discretization, we write the semi-discrete scheme compactly as

$$\frac{\mathrm{d}}{\mathrm{d}t}\boldsymbol{U}(t) = \boldsymbol{\mathcal{L}}(\boldsymbol{U}(t)), \quad \boldsymbol{\mathcal{L}}\big(\boldsymbol{U}(t)\big) = \big(\mathcal{L}_{\boldsymbol{j}}(\boldsymbol{U}(t))\big)_{\boldsymbol{j} \in J},$$

where we define

$$\mathcal{L}_{\boldsymbol{j}}(\boldsymbol{U}(t)) := \frac{1}{h}\sum_{i=1}^{d}\Big(\hat{\boldsymbol{f}}^i_{\boldsymbol{j}+\frac{1}{2}\boldsymbol{e}_i}\big(\boldsymbol{U}(t)\big) - \hat{\boldsymbol{f}}^i_{\boldsymbol{j}-\frac{1}{2}\boldsymbol{e}_i}\big(\boldsymbol{U}(t)\big)\Big)$$

(with suitable modifications for boundary points). For the time discretization, we use the third-order Runge-Kutta TVD scheme proposed in [13].

Assuming that $\boldsymbol{U}^n := \boldsymbol{U}(t^n)$ is given and $\boldsymbol{U}^{n+1} = \boldsymbol{U}(t^{n+1})$ is sought, where $t^{n+1} = t^n + \Delta t$, this scheme is defined as follows:

$$\boldsymbol{U}^{(1)} = \boldsymbol{U}^n - \Delta t \boldsymbol{\mathcal{L}}(\boldsymbol{U}^n),$$
$$\boldsymbol{U}^{(2)} = \frac{3}{4}\boldsymbol{U}^n + \frac{1}{4}\boldsymbol{U}^{(1)} - \frac{1}{4}\Delta t \boldsymbol{\mathcal{L}}(\boldsymbol{U}^{(1)}),$$
$$\boldsymbol{U}^{n+1} = \frac{1}{3}\boldsymbol{U}^n + \frac{2}{3}\boldsymbol{U}^{(2)} - \frac{2}{3}\Delta t \boldsymbol{\mathcal{L}}(\boldsymbol{U}^{(2)}).$$

3 Central weighted essentially nonoscillatory (CWENO) scheme

3.1 Motivation

To motivate the novel approach, which can be considered as an alternative CWENO scheme, let us focus on $d = 1$ space dimension, and for ease of notation on a scalar equation ($m = 1$). We drop the t-dependence of u for simplicity.

The key ingredient for obtaining highly accurate schemes for hyperbolic conservation is the use of reconstructions that, given some contiguous cell-averages of an assumedly unknown function, produce precise local evaluations. For classical finite volume schemes, the reconstructions act on the evolved cell-averages of the solution to precisely approximate the values of the solution at cell-interfaces, whereas for finite difference schemes [14] the reconstructions are applied to split-fluxes to obtain at the end highly accurate approximations to flux derivatives in conservative form.

Assume now that $f_{j-r}, \ldots, f_{j+r}$ are cell-averages associated to a stencil of $2r+1$ points, such that

$$f_{j+l} = \frac{1}{h} \int_{x_{j+l-1/2}}^{x_{j+l+1/2}} f(x)\, dx, \quad l = -r, \ldots, r,$$

and one wishes to obtain an approximation

$$\hat{f}_{j+\tau} = f(x_{j+\tau}) + \mathcal{O}(h^{2r+1}) \quad \text{for } 0 \leq \tau < 1,$$

taking into account as well the eventual presence of discontinuities in the data from the stencil. The case $\tau = 1/2$ is well known and is handled properly by the traditional WENO schemes [7], originally proposed in [9]. The general case of τ is more complicated, since then the ideal weights do not satisfy the same favourable properties as for $\tau = 1/2$. Let us analyze the particular case of our interest, which is $r = 2$ (namely, a fifth-order scheme), for cell-average reconstructions. The three polynomials of degree 2 that interpolate three successive points of the stencil, and whose evaluations at $x_{j+\tau} = x_j + h\tau$ are to be weighted within the WENO reconstruction, are given by

$$p_{0,j}(x_{j+\tau}) = \frac{-1 + 12\tau + 12\tau^2}{24} f_{j-2} + \frac{1 - 24\tau - 12\tau^2}{6} f_{j-1} + \frac{23 + 36\tau + 12\tau^2}{24} f_j,$$

$$p_{1,j}(x_{j+\tau}) = \frac{-1 - 12\tau + 12\tau^2}{24} f_{j-1} + \frac{13 - 12\tau^2}{6} f_j + \frac{-1 + 12\tau + 12\tau^2}{24} f_{j+1},$$

$$p_{2,j}(x_{j+\tau}) = \frac{23 - 36\tau + 12\tau^2}{24} f_j + \frac{1 + 24\tau - 12\tau^2}{6} f_{j+1} + \frac{-1 - 12\tau + 12\tau^2}{24} f_{j+2}.$$

On the other hand, the result of interpolating on the whole stencil of five points and evaluating the resulting polynomial of degree 4 at $x_{j+\tau}$ is

$$\begin{aligned}
p_j(x_{j+\tau}) = &\frac{9 + 200\tau - 120\tau^2 - 160\tau^3 + 80\tau^4}{1920} f_{j-2} \\
&+ \frac{-29 - 340\tau + 360\tau^2 + 80\tau^3 - 80\tau^4}{480} f_{j-1} \\
&+ \frac{1067 - 1320\tau^2 + 240\tau^4}{960} f_j \\
&+ \frac{-29 + 340\tau + 360\tau^2 - 80\tau^3 - 80\tau^4}{480} f_{j+1} \\
&+ \frac{9 - 200\tau - 120\tau^2 + 160\tau^3 + 80\tau^4}{1920} f_{j+2}.
\end{aligned}$$

The ideal weights $c_0(\tau)$, $c_1(\tau)$ and $c_2(\tau)$ are rational expressions in τ for which

$$c_0(\tau) p_0(x_{j+\tau}) + c_1(\tau) p_1(x_{j+\tau}) + c_2(\tau) p_2(x_{j+\tau}) = p(x_{j+\tau}).$$

In this case, we obtain

$$c_0(\tau) = \frac{9 + 200\tau - 120\tau^2 - 160\tau^3 + 80\tau^4}{-80 + 960\tau + 960\tau^2},$$

$$c_1(\tau) = \frac{49 - 4548\tau^2 + 5360\tau^4 - 960\tau^6}{40 - 6720\tau + 5760\tau^2},$$

$$c_2(\tau) = \frac{9 - 200\tau - 120\tau^2 + 160\tau^3 + 80\tau^4}{-80 - 960\tau + 960\tau^2}.$$

Unfortunately, the ideal weights do not behave well for $0 \leq \tau \leq 1$, in the sense that they not only do not satisfy the property $0 \leq c_i(\tau) \leq 1$, but also are unbounded inside such range of $0 \leq \tau < 1$, which makes them unusable in practice.

One can readily check that, for instance, c_0 has a pole at $\tau = -\frac{1}{2} + \frac{\sqrt{3}}{3} \approx 0.07$. However, we must point out that there are values τ which attain the desired properties involving $c_i(\tau)$, such as for $\tau = 1/2$, corresponding to the ideal linear weights associated to the classical WENO schemes

3.2 New formulation

The previous discussion related to the shortcomings of ideal weights motivates a new strategy to design weights for WENO reconstructions. This strategy is to attain the optimal order, $2r + 1$, when the stencil contains smooth data, and to reduce to r-th order when there is some discontinuity in the data. To this end, we utilize the same smoothness indicators $I_{i,j}$ as those defined in [7], namely

$$I_{i,j} = \sum_{k=1}^{r} \int_{x_{j-1/2}}^{x_{j+1/2}} h^{2k-1} \big(p_i^{(k)}(x)\big)^2 \, \mathrm{d}x, \quad 0 \leq i \leq r.$$

We utilize the global average weight as defined in [2], namely

$$\omega_j = \frac{(r+1)^2}{\left(\displaystyle\sum_{i=0}^{r}(I_i + \varepsilon)^m\right)\left(\displaystyle\sum_{i=0}^{r}\frac{1}{(I_i + \varepsilon)^m}\right)}, \quad m > 0, \tag{3.1}$$

where $\varepsilon > 0$ is a small number to avoid divisions by zero. Moreover, loss of accuracy at smooth extrema is also avoided if one sets $\varepsilon = \mathcal{O}(h^2)$. By [2, Prop. 2], ω_j satisfies $0 \leq \omega_j \leq 1$ and, moreover, $\omega_j = 1 - \mathcal{O}(h^{2r})$ if the data from the stencil is smooth enough (assuming $\varepsilon = \mathcal{O}(h^2)$) and $\omega = \mathcal{O}(h^{2m})$ if there is a discontinuity.

Combining properly the weight ω_j defined by (3.1) with the $r + 1$ polynomials of degree r, namely $p_{i,j}$ for $i = 0, \ldots, r$, and the polynomial associated to the whole stencil of degree $2r + 1$, p_j, one can define the *reconstructed value* as

$$\hat{f}_{j+\tau} = \omega_j p_i(x_{j+\tau}) + (1 - \omega_j)q_j(x_{j+\tau}), \quad \text{where} \quad q_j(x_{j+\tau}) := \sum_{i=0}^{r} \omega_{i,j} p_{i,j}(x_{j+\tau})$$

and the so-called *subweights* are defined by

$$\omega_{i,j} := \frac{\alpha_{i,j}}{\alpha_{0,j} + \cdots + \alpha_{r,j}}, \quad \alpha_{k,j} := \frac{c_k}{(I_{k,j} + \varepsilon)^s}, \quad s > 0, \tag{3.2}$$

where the constants c_k can be chosen such that $0 < c_k < 1$ and $c_0 + \cdots + c_r = 1$. This fact is the essential property of the so-called Central WENO schemes, proposed in [8], since, as pointed out in [3], and extrapolating now the claim for reconstructions of arbitrary order, the set of ideal weights in this case is now imposed only by the condition $c_0 + \cdots + c_r = 1$, rather than the much more restrictive condition

$$\sum_{i=0}^{r} c_i p_{i,j}(x_{j+1/2}) = p_i(x_{j+1/2}).$$

For instance, one can simply choose $c_k = \frac{1}{r+1}$ (arithmetic average) or the ideal weights of the case $\tau = 1/2$ (the classical WENO schemes), which satisfy the required properties for any r. By all the above considerations, one can easily show that

$$\hat{f}_{j+\tau} = f(x_{j+\tau}) + \mathcal{O}(h^{2r+1})$$

if there is smoothness and $\varepsilon = \mathcal{O}(h^2)$, and that

$$\hat{f}_{j+\tau} = f(x_{j+\tau}) + \mathcal{O}(h^{r+1})$$

otherwise. As for our choice for the fifth-order scheme (with $r = 2$), we set c_i to be the arithmetic average, namely, $c_0 = c_1 = c_2 = \frac{1}{3}$. Regarding the Jiang-Shu smoothness indicators, they are:

$$I_{0,j} = \frac{1}{3}\big((4f_{j-2} - 19f_{j-1} + 11f_j)f_{j-2} + (25f_{j-1} - 31f_j)f_{j-1} + (10f_j)f_j\big),$$

$$I_{1,j} = \frac{1}{3}\big((4f_{j-1} - 13f_j + 5f_{j+1})f_{j-1} + (13f_j - 13f_{j+1})f_j + (4f_{j+1})f_{j+1}\big),$$

$$I_{2,j} = \frac{1}{3}\big((10f_j - 31f_{j+1} + 11f_{j+2})f_j + (25f_{j+1} - 19f_{j+2})f_{j+1} + (4f_{j+2})f_{j+2}\big).$$

3.3 Accuracy analysis

We next study in full detail the accuracy of the reconstruction described in Section 3.2, focusing in terms of the choice of ε and the number of consecutive derivatives of f, starting by the first one, that vanishes. This will be done through a proper discussion of the parameters m and s that appear in (3.1) and (3.2), respectively. In the case that ε in (3.1) is chosen such that $\varepsilon = \mathcal{O}(h^2)$, the number of vanishing derivatives of f does not have any impact on ω_j or $\omega_{i,j}$, $0 \le i \le r$ (see [1] for further details), since these quantities unconditionally satisfy

$$\omega_j = \begin{cases} 1 - \mathcal{O}(h^{2r}) & \text{if the stencil is smooth,} \\ \mathcal{O}(h^{2m}) & \text{if a discontinuity crosses the stencil,} \end{cases}$$

$$\omega_{i,j} = \begin{cases} \mathcal{O}(1) & \text{if the corresponding substencil is smooth,} \\ \mathcal{O}(h^{2s}) & \text{if a discontinuity crosses the corresponding substencil.} \end{cases}$$

Therefore, taking into account that $\omega_{0,j} + \cdots + \omega_{r,j} = 1$, one has

$$q_j(x_{j+\tau}) = \begin{cases} f(x_{j+\tau}) + \mathcal{O}(h^{r+1}) & \text{if the stencil is smooth,} \\ f(x_{j+\tau}) + \mathcal{O}(h^a) & \text{if a discontinuity crosses the stencil,} \end{cases}$$

where $a = \min\{2s, r+1\}$. Therefore, to attain the optimal order in the latter case, $r+1$, it suffices to take

$$s = \left\lceil \frac{r+1}{2} \right\rceil. \tag{3.3}$$

Finally,

$$\hat{f}_{j+\tau} \begin{cases} f(x_{j+\tau}) + \mathcal{O}(h^{2r+1}) & \text{if the stencil is smooth,} \\ f(x_{j+\tau}) + \mathcal{O}(h^b) & \text{if a discontinuity crosses the stencil,} \end{cases}$$

where $b = \min\{2m, r+1\}$. Thus, to achieve the optimal order in the latter case as well, $r+1$, one can set $m = \lceil (r+1)/2 \rceil$.

Alternatively, one may set the parameter ε in (3.1) to a fixed very small quantity to prevent divisions by zero, and which can be thus neglected in the accuracy analysis. In this case, we must take into account the impact of the smooth extrema in the accuracy of the weights, which is analyzed next. Then, it is convenient to remap accordingly the weight ω_j as

$$\omega_j = (1 - (1 - \rho_j)^{s_1})^{s_2}, \quad \text{where we define} \quad \rho_j := \frac{(r+1)^2}{\left(\displaystyle\sum_{i=0}^{r} (I_i + \varepsilon) \right) \left(\displaystyle\sum_{i=0}^{r} \frac{1}{I_i + \varepsilon} \right)}.$$

Under these conditions, and assuming that k_0 is the maximum order of consecutive vanishing derivatives, namely, such that the k-th derivative of $f(u)$ vanishes at $x_{j+\tau}$, for $1 \le k \le k_0$, but the $(k_0 + 1) - th$ derivative does not, i.e.,

$$\frac{\mathrm{d}^k}{\mathrm{d}x^k} f(u)\Big|_{x_{j+\tau}} = 0, \quad 1 \le k \le k_0; \quad \frac{\mathrm{d}^{k_0+1}}{\mathrm{d}x^{k_0+1}} f(u)\Big|_{x_{j+\tau}} \ne 0$$

then invoking once again [2, Prop. 2] and defining $k_1 := \max\{r - k_0, 0\}$, we get

$$\omega_j = \begin{cases} 1 - \mathcal{O}(h^{2k_1 s_1}) & \text{if the stencil is smooth,} \\ \mathcal{O}(h^{2s_2}) & \text{if a discontinuity crosses the stencil.} \end{cases}$$

It should be noted that in the case where $k_0 \ge r$, then $k_1 = 0$, and ω_j does not approximate 1, yielding an unavoidable loss of accuracy. We next show that otherwise, namely, when $k_0 < r$, then optimal accuracy both in case of smoothness, that is, of order $2r+1$, and in case of a discontinuity in the stencil, of order $r+1$, can be recovered by setting properly s_1 and s_2. Indeed, by setting as in the previous case the parameter of the weights $\omega_{i,j}$, namely, s given by (3.3), we have that

$$q(x_{j+\tau}) = f(x_{j+\tau}) + \mathcal{O}(h^{r+1}),$$

whether the stencil is smooth or not.

On the other hand, taking into consideration the above remarks, we have the following. If there is smoothness, then

$$\begin{aligned} \hat{f}_{j+\tau} &= \omega_j p_j(x_{j+\tau}) + (1 - \omega_j) q_j(x_{j+\tau}) \\ &= (1 - \omega_j)\big(f(x_{j+\tau}) + \mathcal{O}(h^{2r+1}) \big) + \omega_j \big(f(x_{j+\tau}) + \mathcal{O}(h^{r+1}) \big) \\ &= f(x_{j+\tau}) + (1 - \omega_j)\mathcal{O}(h^{2r+1}) + \omega_j \mathcal{O}(h^{r+1}) \end{aligned}$$

$$= f(x_{j+\tau}) + \left(1 - \mathcal{O}(h^{2k_1 s_1})\right)\mathcal{O}(h^{2r+1}) + \mathcal{O}(h^{2k_1 s_1})\mathcal{O}(h^{r+1})$$
$$= f(x_{j+\tau}) + \mathcal{O}(h^{2r+1}) + \mathcal{O}(h^{2k_1 s_1 + r + 1}).$$

Thus, to achieve a $(2r+1)$-th accuracy order, one should impose

$$2k_1 s_1 + r + 1 \geq 2r + 1 \iff s_1 \geq \frac{r}{2k_1}.$$

Finally, since the worst-case scenario under the assumption $k_0 < r$ is $k_0 = r - 1$, namely, $k_1 = 1$, then the optimal exponent choice is $s_1 = \lceil r/2 \rceil$. On the other hand, if there is a discontinuity, following the same reasoning as in the previous cases, the optimal parameter in this case is $s_2 = \lceil (r+1)/2 \rceil$.

Finally, it is worth mentioning that a classical WENO scheme of order $2r + 1$ has actually order $r + 1 + |r - k|$, with $k = \min\{l \geq 1 \mid f^{(l)}(x_{j+1/2}) \neq 0\} - 1$. Therefore, if we take into account our theoretical considerations, for $0 < k < r$ the accuracy order of our scheme is the optimal, namely, $2r + 1$, whereas the accuracy order of the classical WENO schemes in that case is $2r + 1 - k$, and hence under these conditions the latter will have lower accuracy than the former.

4 Numerical experiments

The numerical experiments that will be presented next are divided into two groups. In order to illustrate that the good behaviour of our procedure is agnostic about the type of reconstructions to be weighted, we will use different type of reconstructions in each of these groups.

The first group of numerical experiments is devoted to algebraic problems where we test the performance of our CWENO method both on smooth problems and on discontinuous problems. In this case, the type of reconstructions used are those interpreting the data from stencil as pointwise values of a certain unknown function f. These experiments will be performed in Subsection 4.1.

As for the second group of numerical experiments, they are shown in Subsection 4.2 and involve numerical solutions of hyperbolic conservation laws through the Shu-Osher finite-difference method [13,14], and thus, in this case the data from the stencils is interpreted as cell averages of some unknown function $f(u)$.

4.1 Accuracy tests

Some numerical tests, where we stress out the performance of our scheme against the classical WENO schemes counterpart, will be presented next. These tests will be especially focused on the quantitative behaviour in presence of smooth extrema and discontinuities. To do so, we use an arbitrary precision library, MPFR [10], using its C++ wrapper [6], by setting a precision of 333 bits (≈ 100 digits).

Example 1: Smooth extrema analysis

Let us consider the family of functions $f_k : \mathbb{R} \to \mathbb{R}$, $k \in \mathbb{N}$, given by

$$f_k(x) = x^{k+1}e^x.$$

$r = 1$	WENO3				CWENO3			
	$k = 0$		$k = 1$		$k = 0$		$k = 1$	
n	Error	Order	Error	Order	Error	Order	Error	Order
5	5.11e-03	—	1.00e-02	—	3.33e-04	—	1.00e-02	—
10	6.06e-04	3.07	2.50e-03	2.00	1.46e-04	1.18	2.50e-03	2.00
20	7.32e-05	3.05	6.25e-04	2.00	2.19e-05	2.74	6.25e-04	2.00
40	8.97e-06	3.03	1.56e-04	2.00	2.86e-06	2.93	1.56e-04	2.00
80	1.11e-06	3.01	3.91e-05	2.00	3.63e-07	2.98	3.91e-05	2.00
160	1.38e-07	3.01	9.77e-06	2.00	4.56e-08	2.99	9.77e-06	2.00
320	1.72e-08	3.00	2.44e-06	2.00	5.71e-09	3.00	2.44e-06	2.00
640	2.15e-09	3.00	6.10e-07	2.00	7.15e-10	3.00	6.10e-07	2.00
1280	2.68e-10	3.00	1.53e-07	2.00	8.94e-11	3.00	1.53e-07	2.00

Table 1: Error table for WENO3 and CWENO3 for Example 1. In this case, both methods have the same accuracy for all the cases considered (both dropping to second order when $k = 1$), accordingly to the previous theoretical considerations.

Then f_k has a smooth extreme at $x = 0$ of order k.

We now perform several tests involving different values of k and r, where in each case the corresponding CWENO scheme with $\varepsilon = 10^{-100}$ (negligible) and optimal parameters, $s_1 = \lceil r/2 \rceil$, $s_2 = \lceil (r+1)/2 \rceil$, is compared against the classical WENO scheme of the same order, also with $\varepsilon = 10^{-100}$. In all cases, we define the following stencil:

$$x_j = \left(j - \frac{1}{2} \right) h, \quad -r \leq j \leq r,$$

and perform the reconstruction at $x = 0$ for different values of $h > 0$. Since in this case one has a centered reconstruction point, we use the same ideal weights of the traditional WENO schemes to define the subweights. In this case, since the reconstructions are performed in the classical sense, namely, $\tau = 1/2$, we choose as the non-linear subweights for the CWENO schemes those based on the ideal linear weights. We will perform accuracy tests for $1 \leq r \leq 4$, namely, from (C)WENO3 to (C)WENO9, using the reconstructions from pointwise values to pointwise values, choosing in each case the lowest possible exponents, s_1, s_2, to attain the optimal order discussed before, that is, $s_1 = \lceil r/2 \rceil$ and $s_2 = \lceil (r+1)/2 \rceil$. Assuming $h = 1/n$, $n \in \mathbb{N}$, the results are shown in Tables 1–4, where the error is $|P(0) - f_k(0)|$, where $P(0)$ denotes the corresponding reconstruction from pointwise values to pointwise values at $x = 0$.

According to the tables, one can conclude that the numerical results agree with the theoretical considerations.

Example 2: Discontinuous data analysis

We next consider instead the function $g : \mathbb{R} \to \mathbb{R}$ given by

$$g(x) = \begin{cases} e^x & x \leq 0, \\ e^{x+1} & x > 0, \end{cases}$$

and perform the accuracy tests for $1 \leq r \leq 4$ with the same setup as the previous case. Results are shown in Tables 5–6.

	$r = 2$	$k = 0$		$k = 1$		$k = 2$	
	n	Error	Order	Error	Order	Error	Order
WENO5	5	1.52e-04	—	2.02e-04	—	1.90e-03	—
	10	6.67e-06	4.51	1.34e-06	7.23	2.08e-04	3.20
	20	2.29e-07	4.86	1.37e-06	-0.03	1.97e-05	3.40
	40	7.35e-09	4.96	1.44e-07	3.25	1.90e-06	3.37
	80	2.31e-10	4.99	1.09e-08	3.72	1.98e-07	3.27
	160	7.25e-12	5.00	7.44e-10	3.88	2.21e-08	3.16
	320	2.27e-13	5.00	4.84e-11	3.94	2.60e-09	3.09
	640	7.09e-15	5.00	3.08e-12	3.97	3.14e-10	3.05
	1280	2.22e-16	5.00	1.95e-13	3.99	3.86e-11	3.02
	2560	6.93e-18	5.00	1.22e-14	3.99	4.78e-12	3.01
	5120	2.16e-19	5.00	7.66e-16	4.00	5.95e-13	3.01
	10240	6.77e-21	5.00	4.79e-17	4.00	7.42e-14	3.00
	20480	2.11e-22	5.00	3.00e-18	4.00	9.26e-15	3.00
	40960	6.61e-24	5.00	1.87e-19	4.00	1.16e-15	3.00
CWENO5	5	1.91e-05	—	1.51e-04	—	7.86e-04	—
	10	5.62e-07	5.09	1.99e-06	6.25	1.15e-04	2.78
	20	1.79e-08	4.97	3.64e-08	5.77	1.35e-05	3.09
	40	5.65e-10	4.98	6.16e-10	5.88	1.42e-06	3.25
	80	1.78e-11	4.99	1.61e-11	5.26	1.53e-07	3.21
	160	5.57e-13	5.00	1.29e-12	3.64	1.74e-08	3.14
	320	1.74e-14	5.00	5.45e-14	4.57	2.06e-09	3.08
	640	5.45e-16	5.00	1.94e-15	4.81	2.50e-10	3.04
	1280	1.70e-17	5.00	6.43e-17	4.91	3.08e-11	3.02
	2560	5.33e-19	5.00	2.07e-18	4.96	3.82e-12	3.01
	5120	1.67e-20	5.00	6.57e-20	4.98	4.76e-13	3.01
	10240	5.20e-22	5.00	2.07e-21	4.99	5.94e-14	3.00
	20480	1.63e-23	5.00	6.48e-23	4.99	7.41e-15	3.00
	40960	5.08e-25	5.00	2.03e-24	5.00	9.26e-16	3.00

Table 2: Error table for WENO5 and CWENO5 for Example 1. The gradual loss of accuracy as k increases can be clearly seen in the case of WENO5, whereas CWENO5 keeps the optimal accuracy order for $k < 2$.

From the results it can be concluded that the order in presence of discontinuities is the optimal through the indicated choices for the parameters s_1 and s_2. This feature is thus shared by the classical WENO schemes with the suitable choice of the parameter s.

Example 3: Non-aligned stencil with smooth data

We now consider again the setup as in Example 1, with the difference that now the stencil is based on the following grid points, which are based on choosing the displacement parameter $\tau = 3/4$:

$$x_j = \left(j - \frac{3}{4}\right) h, \quad -r \le j \le r.$$

Since we want to interpolate at $x = 0$, in this case the stencil is displaced with respect to x, and thus the classical WENO procedure cannot provide a satisfactory procedure to solve this problem, whereas our approach is able to by just choosing, for instance, the subweights based on the uniform ideal weights, as it can be seen in Tables 7–10.

	$r = 3$	$k = 0$		$k = 1$		$k = 2$		$k = 3$	
	n	Error	Order	Error	Order	Error	Order	Error	Order
WENO7	5	1.91e-06	—	7.10e-06	—	7.40e-04	—	9.20e-04	—
	10	2.19e-08	6.44	9.44e-07	2.91	2.16e-05	5.10	5.65e-05	4.03
	20	1.92e-10	6.84	1.27e-08	6.22	3.76e-07	5.84	3.51e-06	4.01
	40	1.55e-12	6.96	1.59e-10	6.32	5.48e-09	6.10	2.19e-07	4.00
	80	1.22e-14	6.99	2.12e-12	6.22	6.53e-11	6.39	1.37e-08	4.00
	160	9.54e-17	7.00	3.04e-14	6.13	3.28e-13	7.64	8.54e-10	4.00
	320	7.46e-19	7.00	4.52e-16	6.07	1.70e-14	4.27	5.34e-11	4.00
	640	5.83e-21	7.00	6.89e-18	6.04	9.61e-16	4.15	3.34e-12	4.00
	1280	4.55e-23	7.00	1.06e-19	6.02	3.68e-17	4.71	2.09e-13	4.00
	2560	3.56e-25	7.00	1.65e-21	6.01	1.25e-18	4.87	1.30e-14	4.00
	5120	2.78e-27	7.00	2.57e-23	6.00	4.09e-20	4.94	8.15e-16	4.00
	10240	2.17e-29	7.00	4.01e-25	6.00	1.30e-21	4.97	5.09e-17	4.00
	20480	1.70e-31	7.00	6.26e-27	6.00	4.11e-23	4.99	3.18e-18	4.00
	40960	1.33e-33	7.00	9.78e-29	6.00	1.29e-24	4.99	1.99e-19	4.00
	81920	1.04e-35	7.00	1.53e-30	6.00	4.04e-26	5.00	1.24e-20	4.00
CWENO7	5	2.00e-07	—	1.22e-06	—	5.42e-04	—	8.93e-04	—
	10	1.63e-09	6.94	9.71e-09	6.97	4.29e-06	6.98	5.34e-05	4.06
	20	1.30e-11	6.97	7.79e-11	6.96	9.32e-09	8.85	3.32e-06	4.01
	40	1.03e-13	6.98	6.17e-13	6.98	1.36e-11	9.42	2.09e-07	3.99
	80	8.10e-16	6.99	4.85e-15	6.99	3.29e-14	8.69	1.31e-08	4.00
	160	6.35e-18	7.00	3.81e-17	6.99	1.93e-16	7.41	8.19e-10	4.00
	320	4.97e-20	7.00	2.98e-19	7.00	1.48e-18	7.03	5.12e-11	4.00
	640	3.88e-22	7.00	2.33e-21	7.00	1.16e-20	6.99	3.20e-12	4.00
	1280	3.03e-24	7.00	1.82e-23	7.00	9.09e-23	7.00	2.00e-13	4.00
	2560	2.37e-26	7.00	1.42e-25	7.00	7.11e-25	7.00	1.25e-14	4.00
	5120	1.85e-28	7.00	1.11e-27	7.00	5.56e-27	7.00	7.83e-16	4.00
	10240	1.45e-30	7.00	8.68e-30	7.00	4.34e-29	7.00	4.89e-17	4.00
	20480	1.13e-32	7.00	6.79e-32	7.00	3.39e-31	7.00	3.06e-18	4.00
	40960	8.84e-35	7.00	5.30e-34	7.00	2.65e-33	7.00	1.91e-19	4.00
	81920	6.90e-37	7.00	4.14e-36	7.00	2.07e-35	7.00	1.19e-20	4.00

Table 3: Error table for WENO7 and CWENO7 for Example 1. The gradual loss of accuracy as k increases can be clearly seen in the case of WENO7, whereas CWENO7 keeps the optimal accuracy order for $k < 3$.

The results show that our scheme is also suitable for problems where the reconstruction point is not centered and attains the optimal order as in the centered case.

Example 4: Non-aligned stencil with discontinuous data

Now, we change our setup to the one defined in Example 2, with the stencil arrangement and subweights of Example 3. Results are shown in Table 11.

From the results, it can be concluded that in the case of non-centered reconstruction points the order is also the optimal in presence of discontinuities in the data.

	$r=4$	$k=0$		$k=1$		$k=2$		$k=3$		$k=4$	
	n	Error	Order	Error	Order	Error	Order	Error	Order	Error	Order
WENO9	5	2.98e-08	—	3.86e-06	—	3.10e-05	—	1.74e-04	—	2.80e-04	—
	10	1.24e-10	7.91	1.22e-08	8.31	4.28e-07	6.18	6.32e-06	4.78	9.97e-06	4.81
	20	2.78e-13	8.80	3.40e-11	8.49	2.09e-09	7.68	7.23e-08	6.45	2.07e-07	5.59
	40	5.61e-16	8.95	1.00e-13	8.40	7.02e-12	8.22	3.66e-10	7.63	1.70e-09	6.93
	80	1.11e-18	8.99	3.26e-16	8.27	3.03e-14	7.86	8.24e-13	8.80	3.88e-11	5.45
	160	2.17e-21	9.00	1.14e-18	8.16	1.68e-16	7.49	3.20e-15	8.01	2.64e-12	3.88
	320	4.23e-24	9.00	4.19e-21	8.09	1.10e-18	7.26	4.95e-17	6.01	1.04e-13	4.67
	640	8.27e-27	9.00	1.59e-23	8.05	7.83e-21	7.13	2.05e-19	7.91	3.58e-15	4.86
	1280	1.62e-29	9.00	6.10e-26	8.02	5.86e-23	7.06	3.57e-21	5.85	1.17e-16	4.94
	2560	3.16e-32	9.00	2.36e-28	8.01	4.48e-25	7.03	1.18e-22	4.92	3.73e-18	4.97
	5120	6.16e-35	9.00	9.20e-31	8.01	3.46e-27	7.02	2.37e-24	5.64	1.18e-19	4.98
	10240	1.20e-37	9.00	3.59e-33	8.00	2.69e-29	7.01	4.12e-26	5.84	3.70e-21	4.99
	20480	2.35e-40	9.00	1.40e-35	8.00	2.09e-31	7.00	6.78e-28	5.93	1.16e-22	5.00
	40960	4.59e-43	9.00	5.46e-38	8.00	1.63e-33	7.00	1.09e-29	5.96	3.63e-24	5.00
	81920	8.97e-46	9.00	2.13e-40	8.00	1.28e-35	7.00	1.72e-31	5.98	1.14e-25	5.00
	163840	1.75e-48	9.00	8.33e-43	8.00	9.96e-38	7.00	2.70e-33	5.99	3.55e-27	5.00
	327680	3.42e-51	9.00	3.25e-45	8.00	7.78e-40	7.00	4.23e-35	6.00	1.11e-28	5.00
	655360	6.68e-54	9.00	1.27e-47	8.00	6.08e-42	7.00	6.62e-37	6.00	3.47e-30	5.00
CWENO9	5	2.26e-09	—	1.71e-08	—	9.48e-06	—	1.73e-04	—	2.80e-04	—
	10	4.59e-12	8.94	3.65e-11	8.87	4.84e-10	14.26	4.39e-06	5.30	9.77e-06	4.84
	20	9.16e-15	8.97	7.31e-14	8.96	5.19e-13	9.86	1.14e-08	8.60	1.93e-07	5.66
	40	1.81e-17	8.98	1.45e-16	8.98	1.01e-15	9.00	6.13e-12	10.86	1.58e-09	6.93
	80	3.56e-20	8.99	2.85e-19	8.99	1.99e-18	8.99	1.07e-15	12.49	3.65e-11	5.44
	160	6.97e-23	9.00	5.58e-22	8.99	3.90e-21	8.99	3.11e-19	11.74	2.50e-12	3.87
	320	1.36e-25	9.00	1.09e-24	9.00	7.63e-24	9.00	3.36e-22	9.86	9.88e-14	4.66
	640	2.67e-28	9.00	2.13e-27	9.00	1.49e-26	9.00	1.66e-25	10.98	3.41e-15	4.86
	1280	5.21e-31	9.00	4.17e-30	9.00	2.92e-29	9.00	9.10e-29	10.83	1.11e-16	4.93
	2560	1.02e-33	9.00	8.14e-33	9.00	5.70e-32	9.00	1.67e-31	9.09	3.56e-18	4.97
	5120	1.99e-36	9.00	1.59e-35	9.00	1.11e-34	9.00	4.49e-34	8.54	1.12e-19	4.98
	10240	3.88e-39	9.00	3.11e-38	9.00	2.17e-37	9.00	1.07e-36	8.72	3.53e-21	4.99
	20480	7.58e-42	9.00	6.07e-41	9.00	4.25e-40	9.00	2.30e-39	8.85	1.11e-22	5.00
	40960	1.48e-44	9.00	1.18e-43	9.00	8.29e-43	9.00	4.73e-42	8.93	3.46e-24	5.00
	81920	2.89e-47	9.00	2.31e-46	9.00	1.62e-45	9.00	9.48e-45	8.96	1.08e-25	5.00
	163840	5.65e-50	9.00	4.52e-49	9.00	3.16e-48	9.00	1.87e-47	8.98	3.38e-27	5.00
	327680	1.10e-52	9.00	8.83e-52	9.00	6.18e-51	9.00	3.68e-50	8.99	1.06e-28	5.00
	655360	2.16e-55	9.00	1.72e-54	9.00	1.21e-53	9.00	7.22e-53	9.00	3.30e-30	5.00

Table 4: Error table for WENO9 and CWENO9 for Example 1. The gradual loss of accuracy as k increases can be clearly seen in the case of WENO9, whereas CWENO9 keeps the optimal accuracy order for $k < 4$.

4.2 Conservation laws experiments

Example 5. 1D Euler equations: Shu-Osher problem

The 1D Euler equations for gas dynamics are given by (2.1) for $m = 3$ and $d = 1$ with $\boldsymbol{u} = (\rho, \rho v, E)^{\mathrm{T}}$ and $\boldsymbol{f}(\boldsymbol{u}) = \boldsymbol{f}^1(\boldsymbol{u}) = (\rho v, p + \rho v^2, v(E + p))^{\mathrm{T}}$, where ρ is the density, v is the velocity and E is the specific energy of the system. The variable p stands for the pressure and is given by the equation of state

$$p = (\gamma - 1)\left(E - \frac{1}{2}\rho v^2\right),$$

where γ is the adiabatic constant that will be taken as $\gamma = 1.4$. We now consider the interaction with a Mach 3 shock and a sine wave. The spatial domain is now

	WENO3		CWENO3		WENO5		CWENO5	
n	Error	Order	Error	Order	Error	Order	Error	Order
5	4.25e-03	—	2.13e-02	—	1.67e-03	—	1.38e-03	—
10	2.59e-03	0.71	8.65e-03	1.30	2.48e-04	2.75	2.25e-04	2.62
20	9.13e-04	1.50	2.73e-03	1.66	3.45e-05	2.85	3.28e-05	2.78
40	2.68e-04	1.77	7.65e-04	1.83	4.58e-06	2.91	4.47e-06	2.88
80	7.22e-05	1.89	2.02e-04	1.92	5.91e-07	2.95	5.84e-07	2.94
160	1.87e-05	1.95	5.21e-05	1.96	7.51e-08	2.98	7.46e-08	2.97
320	4.77e-06	1.97	1.32e-05	1.98	9.46e-09	2.99	9.43e-09	2.98
640	1.20e-06	1.99	3.32e-06	1.99	1.19e-09	2.99	1.19e-09	2.99
1280	3.03e-07	1.99	8.34e-07	1.99	1.49e-10	3.00	1.49e-10	3.00
2560	7.58e-08	2.00	2.09e-07	2.00	1.86e-11	3.00	1.86e-11	3.00
5120	1.90e-08	2.00	5.23e-08	2.00	2.33e-12	3.00	2.33e-12	3.00

Table 5: Error table for $r = 1$ and $r = 2$, Example 2. It can be seen that the obtained accuracy order is consistent with our theoretical considerations.

	WENO7		CWENO7		WENO9		CWENO9	
n	Error	Order	Error	Order	Error	Order	Error	Order
5	8.43e-06	—	3.53e-04	—	5.20e-05	—	5.13e-05	—
10	2.38e-06	1.82	2.84e-05	3.63	2.00e-06	4.70	1.98e-06	4.69
20	2.97e-07	3.00	2.06e-06	3.78	6.92e-08	4.85	6.90e-08	4.85
40	2.44e-08	3.60	1.40e-07	3.88	2.28e-09	4.92	2.28e-09	4.92
80	1.73e-09	3.82	9.10e-09	3.94	7.31e-11	4.96	7.31e-11	4.96
160	1.15e-10	3.91	5.81e-10	3.97	2.32e-12	4.98	2.32e-12	4.98
320	7.41e-12	3.96	3.67e-11	3.98	7.29e-14	4.99	7.28e-14	4.99
640	4.70e-13	3.98	2.31e-12	3.99	2.28e-15	5.00	2.28e-15	5.00
1280	2.96e-14	3.99	1.44e-13	4.00	7.15e-17	5.00	7.15e-17	5.00
2560	1.86e-15	3.99	9.04e-15	4.00	2.24e-18	5.00	2.24e-18	5.00
5120	1.16e-16	4.00	5.65e-16	4.00	6.99e-20	5.00	6.99e-20	5.00

Table 6: Error table for $r = 3$ and $r = 4$, Example 2. It can be seen that the obtained accuracy order agrees with our theoretical analysis.

$r = 1$	$k = 0$		$k = 1$	
n	Error	Order	Error	Order
5	3.55e-03	—	4.05e-03	—
10	1.17e-04	4.92	1.05e-03	1.95
20	4.17e-06	4.81	2.69e-04	1.97
40	1.59e-06	1.39	6.82e-05	1.98
80	2.61e-07	2.61	1.72e-05	1.99
160	3.64e-08	2.84	4.31e-06	1.99
320	4.78e-09	2.93	1.08e-06	2.00
640	6.12e-10	2.97	2.70e-07	2.00
1280	7.73e-11	2.98	6.75e-08	2.00
2560	9.72e-12	2.99	1.69e-08	2.00
5120	1.22e-12	3.00	4.22e-09	2.00

Table 7: Error table for CWENO3 for Example 3. The results are consistent with our theoretical considerations, attaining the optimal order for $k < 1$.

$r = 2$	$k = 0$		$k = 1$		$k = 2$	
n	Error	Order	Error	Order	Error	Order
5	8.55e-05	—	4.32e-03	—	1.13e-03	—
10	7.23e-07	6.88	2.39e-04	4.18	2.17e-04	2.37
20	1.60e-08	5.50	8.39e-06	4.83	2.84e-05	2.94
40	4.65e-10	5.11	2.62e-07	5.00	3.56e-06	2.99
80	1.43e-11	5.02	8.03e-09	5.03	4.45e-07	3.00
160	4.47e-13	5.00	2.48e-10	5.02	5.56e-08	3.00
320	1.40e-14	5.00	7.68e-12	5.01	6.94e-09	3.00
640	4.37e-16	5.00	2.39e-13	5.01	8.68e-10	3.00
1280	1.37e-17	5.00	7.45e-15	5.00	1.08e-10	3.00

Table 8: Error table for CWENO5 for Example 3. The optimal order is attained for $k < 2$, and thus, the results are consistent with our theoretical analysis.

$r = 3$	$k = 0$		$k = 1$		$k = 2$		$k = 3$	
n	Error	Order	Error	Order	Error	Order	Error	Order
5	1.47e-07	—	5.16e-06	—	7.63e-04	—	3.80e-04	—
10	1.23e-09	6.90	6.76e-09	9.58	2.86e-05	4.74	2.25e-05	4.08
20	9.95e-12	6.95	5.92e-11	6.83	2.37e-07	6.92	1.49e-06	3.91
40	7.92e-14	6.97	4.74e-13	6.97	1.14e-09	7.69	1.00e-07	3.90
80	6.24e-16	6.99	3.74e-15	6.98	4.67e-12	7.94	6.48e-09	3.95
160	4.90e-18	6.99	2.94e-17	6.99	1.83e-14	8.00	4.11e-10	3.98
320	3.84e-20	7.00	2.30e-19	7.00	7.07e-17	8.01	2.59e-11	3.99
640	3.00e-22	7.00	1.80e-21	7.00	2.71e-19	8.03	1.62e-12	3.99
1280	2.35e-24	7.00	1.41e-23	7.00	1.02e-21	8.05	1.02e-13	4.00
2560	1.83e-26	7.00	1.10e-25	7.00	3.71e-24	8.10	6.36e-15	4.00
5120	1.43e-28	7.00	8.60e-28	7.00	1.23e-26	8.23	3.98e-16	4.00
10240	1.12e-30	7.00	6.72e-30	7.00	3.14e-29	8.62	2.49e-17	4.00
20480	8.75e-33	7.00	5.25e-32	7.00	8.65e-33	11.82	1.55e-18	4.00
40960	6.83e-35	7.00	4.10e-34	7.00	1.06e-33	3.03	9.72e-20	4.00
81920	5.34e-37	7.00	3.20e-36	7.00	1.21e-35	6.45	6.07e-21	4.00
163840	4.17e-39	7.00	2.50e-38	7.00	1.10e-37	6.79	3.80e-22	4.00
327680	3.26e-41	7.00	1.96e-40	7.00	9.18e-40	6.90	2.37e-23	4.00
655360	2.55e-43	7.00	1.53e-42	7.00	7.41e-42	6.95	1.48e-24	4.00
1310720	1.99e-45	7.00	1.19e-44	7.00	5.88e-44	6.98	9.27e-26	4.00
2621440	1.55e-47	7.00	9.32e-47	7.00	4.63e-46	6.99	5.79e-27	4.00
5242880	1.21e-49	7.00	7.28e-49	7.00	3.63e-48	6.99	3.62e-28	4.00
10485760	9.48e-52	7.00	5.69e-51	7.00	2.84e-50	7.00	2.26e-29	4.00

Table 9: Error table for CWENO7 for Example 3. The results agree with our theoretical considerations, with optimal order for $k < 3$.

given by $\Omega := (-5, 5) \ni x_1 =: x$, with the initial condition

$$(\rho, v, p)(x, 0) = \begin{cases} (3.857143, 2.629369, 10.33333) & \text{if } x \leq -4, \\ (1.0 + 0.2\sin(5x), 0, 1) & \text{if } x > -4, \end{cases}$$

with left inflow and right outflow boundary conditions.

We run one simulation until $T = 1.8$ and compare the results obtained with the classical WENO5 scheme and the proposed CWENO schemes for $1 \leq s_1 \leq 3$ (let us recall that the smallest parameter to achieve the fifth order accuracy in this case is $r_1 = 1$), $s_2 = 2$ (the smallest parameter to achieve the optimal accuracy in presence of discontinuities), using the subweights based on the classical WENO

$r=4$	$k=0$		$k=1$		$k=2$		$k=3$		$k=4$	
n	Error	Order	Error	Order	Error	Order	Error	Order	Error	Order
5	1.63e-09	—	7.12e-08	—	3.19e-04	—	1.26e-04	—	3.77e-04	—
10	3.39e-12	8.91	2.71e-11	11.36	1.20e-08	14.69	1.40e-05	3.17	9.07e-06	5.38
20	6.86e-15	8.95	5.46e-14	8.95	3.86e-12	11.61	2.79e-07	5.65	2.93e-07	4.95
40	1.36e-17	8.97	1.09e-16	8.97	1.25e-15	11.60	1.18e-09	7.88	9.07e-09	5.01
80	2.69e-20	8.99	2.15e-19	8.99	1.56e-18	9.64	2.85e-12	8.69	2.81e-10	5.01
160	5.28e-23	8.99	4.22e-22	8.99	2.96e-21	9.05	5.82e-15	8.94	8.76e-12	5.01
320	1.03e-25	9.00	8.26e-25	9.00	5.78e-24	9.00	1.14e-17	9.00	2.73e-13	5.00
640	2.02e-28	9.00	1.62e-27	9.00	1.13e-26	9.00	2.22e-20	9.01	8.52e-15	5.00
1280	3.95e-31	9.00	3.16e-30	9.00	2.21e-29	9.00	4.32e-23	9.00	2.66e-16	5.00

Table 10: Error table for CWENO9 for Example 3. The optimal order is attained for $k < 4$, and therefore the results are again consistent with our theoretical considerations.

	CWENO3		CWENO5		CWENO7		CWENO9	
n	Error	Order	Error	Order	Error	Order	Error	Order
5	1.50e-02	—	3.20e-03	—	4.26e-05	—	1.08e-04	—
10	7.35e-03	1.03	4.84e-04	2.72	3.49e-06	3.61	4.25e-06	4.67
20	2.47e-03	1.57	6.72e-05	2.85	2.22e-07	3.98	1.49e-07	4.83
40	7.12e-04	1.80	8.88e-06	2.92	1.34e-08	4.05	4.94e-09	4.92
80	1.91e-04	1.90	1.14e-06	2.96	8.07e-10	4.05	1.59e-10	4.96
160	4.94e-05	1.95	1.45e-07	2.98	4.94e-11	4.03	5.04e-12	4.98
320	1.26e-05	1.98	1.82e-08	2.99	3.05e-12	4.02	1.59e-13	4.99
640	3.17e-06	1.99	2.29e-09	2.99	1.89e-13	4.01	4.97e-15	4.99
1280	7.95e-07	1.99	2.86e-10	3.00	1.18e-14	4.00	1.56e-16	5.00
2560	1.99e-07	2.00	3.58e-11	3.00	7.36e-16	4.00	4.87e-18	5.00

Table 11: Error table for Example 4. The results are consistent with our theoretical considerations.

ideal weights, $n = 200$ cells, CFL $= 0.5$ with a reference solution computed with 16000 grid points. The results are shown in Figure 1 for the density field.

From the results, one can conclude that the CWENO schemes capture better both the smooth extrema and the discontinuities in the numerical solution, yielding better results as the parameter s_1 increases (namely, when the global average weight involving the spatial reconstructions is closest to 1, thus increasing the impact of the full degree reconstruction polynomial on the reconstruction).

Finally, in order to stress the performance of our new scheme, we also show a comparison between the schemes involving the CPU time versus the error in $\|\cdot\|_1$, which is shown in Figure 2.

Example 6. 2D Euler equations: Double Mach Reflection

The equations that will be considered in this section are the two-dimensional Euler equations for inviscid gas dynamics given by (2.1) for $m = 4$ and $d = 2$, where setting $x = x_1$ and $y = x_2$, we have

$$\boldsymbol{u} = \begin{pmatrix} \rho \\ \rho v^x \\ \rho v^y \\ E \end{pmatrix}, \quad \boldsymbol{f}^1(\boldsymbol{u}) = \begin{pmatrix} \rho v^x \\ p + \rho(v^x)^2 \\ \rho v^x v^y \\ v^x(E+p) \end{pmatrix}, \quad \boldsymbol{f}^2(\boldsymbol{u}) = \begin{pmatrix} \rho v^y \\ \rho v^x v^y \\ p + \rho(v^y)^2 \\ v^y(E+p) \end{pmatrix}.$$

(a) Numerical solution overview

(b) Enlarged view (I)
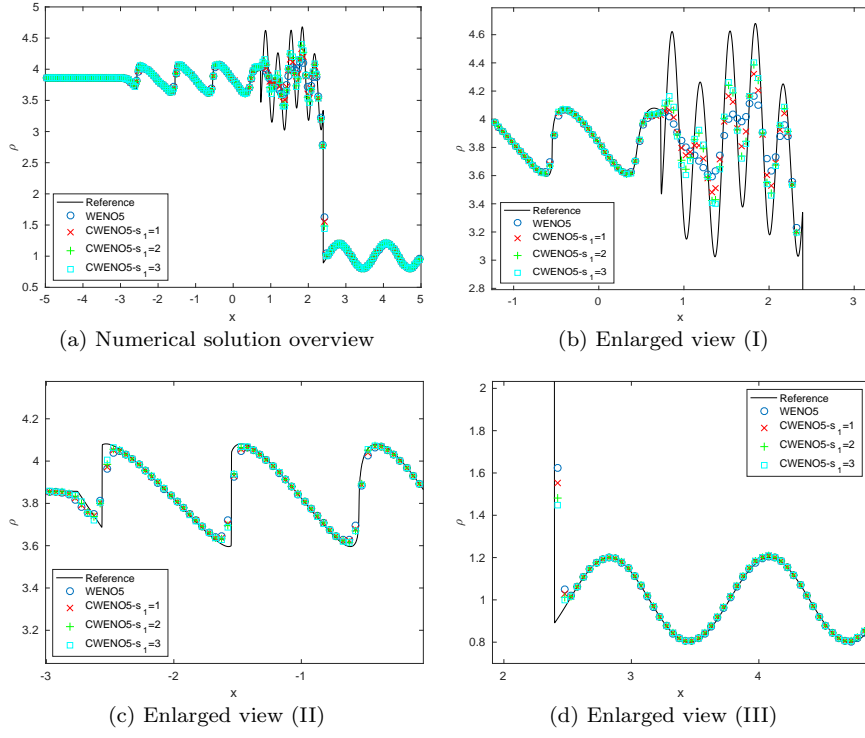
(c) Enlarged view (II)

(d) Enlarged view (III)

Fig. 1: Example 5 (Shu-Osher problem), 200 points, $s_2 = 2$, $T = 1.8$. Density field.
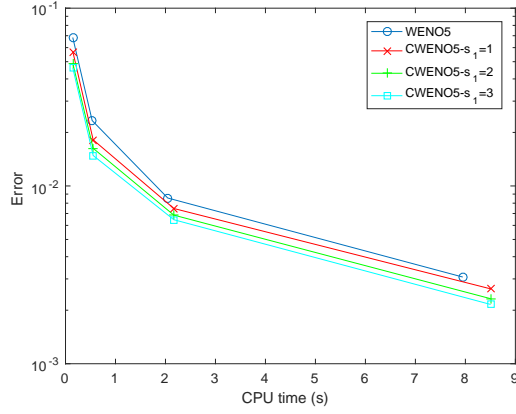

Fig. 2: Example 5 (Shu-Osher problem), CPU comparison.

Here ρ is the density, (v^x, v^y) is the velocity, E is the specific energy, and p is the pressure that is given by the equation of state

$$p = (\gamma - 1)\left(E - \frac{1}{2}\rho((v^x)^2 + (v^y)^2)\right),$$

Schemes/Cost	$r = 1$	$r = 2$	$r = 3$	$r = 4$
WENO	29.156423	47.148631	66.884421	83.571249
CWENO	30.775380	48.400079	68.383047	83.975357
Ratio	1.0555	1.0265	1.0224	1.0048

Table 12: Efficiency table for Example 6 (Double Mach Reflection problem) with a 256×64 points grid (cost in seconds).

where the adiabatic constant is again chosen as $\gamma = 1.4$.

This experiment uses these equations to model a vertical right-going Mach 10 shock colliding with an equilateral triangle. By symmetry, this is equivalent to a collision with a ramp with a slope of $30°$ with respect to the horizontal line.

For the sake of simplicity, we consider the equivalent problem in a rectangle, consisting in a rotated shock, whose vertical angle is $30°$. The domain is the rectangle $\Omega = [0, 4] \times [0, 1]$, whose initial conditions are

$$(\rho, v^x, v^y, E)(x, y, 0) = \begin{cases} \boldsymbol{c}_1 = (\rho_1, v_1^x, v_1^y, E_1) & \text{if } y \leq \frac{1}{4} + \tan(\frac{\pi}{6})x, \\ \boldsymbol{c}_2 = (\rho_2, v_2^x, v_2^y, E_2) & \text{if } \frac{1}{4} + \tan(\frac{\pi}{6})x, \end{cases}$$

$$\boldsymbol{c}_1 = \big(8, 8.25\cos(\pi/6), -8.25\sin(\pi/6), 563.5\big), \quad \boldsymbol{c}_2 = (1.4, 0, 0, 2.5).$$

We impose inflow boundary conditions, with value $\boldsymbol{c}_1$, at the left side, $\{0\} \times [0, 1]$, outflow boundary conditions both at $[0, \frac{1}{4}] \times \{0\}$ and $\{4\} \times [0, 1]$, reflecting boundary conditions at $]\frac{1}{4}, 4] \times \{0\}$ and inflow boundary conditions at the upper side, $[0, 4] \times \{1\}$, which mimics the shock at its actual traveling speed:

$$(\rho, v^x, v^y, E)(x, 1, t) = \begin{cases} \boldsymbol{c}_1 & \text{if } x \leq \frac{1}{4} + \frac{1+20t}{\sqrt{3}}, \\ \boldsymbol{c}_2 & \text{if } x > \frac{1}{4} + \frac{1+20t}{\sqrt{3}}. \end{cases}$$

We run different simulations until $T = 0.2$ both at a resolution of 2048×512 points, shown in Figure 3, and a resolution of 2560×640 points, shown in Figure 4, in both cases with CFL = 0.4 and involving the classical WENO5 scheme and our CWENO schemes with $1 \leq s_1 \leq 3$, $s_2 = 2$, and using the subweights based on the classical WENO ideal weights in the latter case.

From the results, it can be seen that our scheme captures better some features of a complex weak solution, such as turbulence and vorticity. Moreover, and in qualitative terms, the results obtained with a CWENO5 scheme in a resolution of 2048×512 points are similar to those obtained through the classical WENO5 scheme in a resolution of 2560×640 points.

Finally, Table 12 shows a comparison in regards of the computational cost for the corresponding $(2r + 1)$-th schemes, with $1 \leq r \leq 4$, for a resolution of 256×64 points.

5 Conclusions

This paper proposes a novel WENO approach based on the computation of a global average weight as an additional measure of the global smoothness in a stencil. Such weight is then used to confer a stronger control involving the average between a
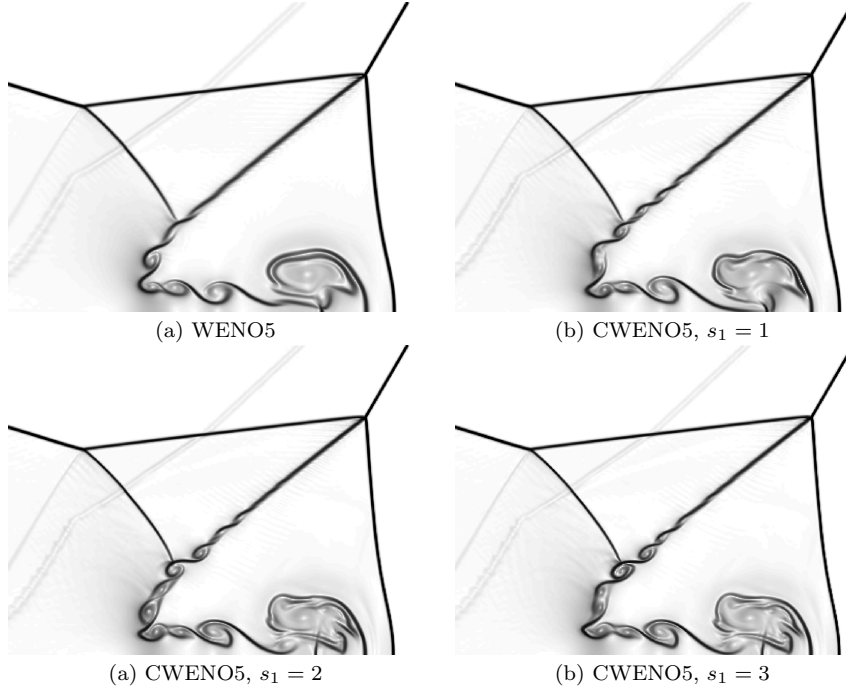
(a) WENO5   (b) CWENO5, $s_1 = 1$

(a) CWENO5, $s_1 = 2$ (b) CWENO5, $s_1 = 3$

Fig. 3: Example 6 (Double Mach Reflection), enlarged view to turbulence zone, 2048×512, $s_2 = 2$, $T = 0.2$ (Schlieren plot).

reconstruction using the whole stencil, which ideally is performed when there is smoothness, and a reconstruction using properly half of the information from a smooth region, ideally performed when there is a discontinuity in the stencil.

We have seen both theoretically and in practice that this approach overcomes whenever possible the well-known issues of the classical WENO schemes involving the loss of accuracy near smooth extrema and handling properly discontinuities, both quantitatively (theoretical results and numerical evidence) and qualitatively (best resolution near smooth extrema and shocks). Moreover, this approach can be used to easily tackle further issues regarding the WENO schemes, such as the presence of negative ideal weights for certain reconstructions (see for instance [12] for further details involving reconstructions with negative weights) and the reconstruction at non-centered points.

Regarding the aforementioned considerations, we plan to use these schemes in several contexts, such as WENO reconstructions of derivatives and as a part of a more accurate boundary extrapolation algorithm, which will be illustrated in forthcoming works.

Acknowledgments

(a) WENO5   (b) CWENO5, $s_1 = 1$
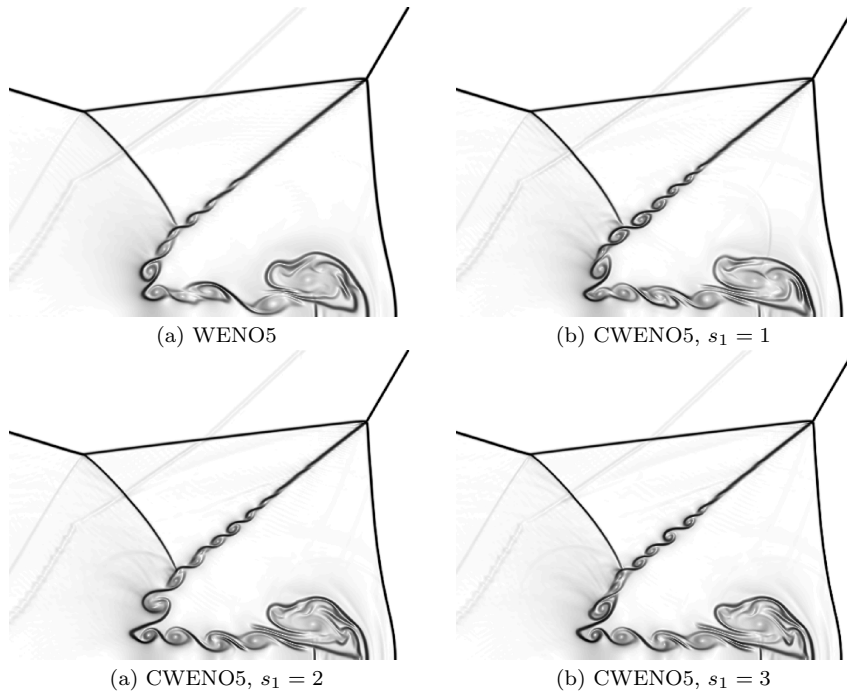
(a) CWENO5, $s_1 = 2$ (b) CWENO5, $s_1 = 3$

Fig. 4: Example 6 (Double Mach Reflection), enlarged view to turbulence zone, 2560×640, $s_2 = 2$, $T = 0.2$ (Schlieren plot).

References

1. Aràndiga, F., Baeza, A., Belda, A.M., Mulet, P.: Analysis of WENO schemes for full and global accuracy. SIAM J. Numer. Anal. **49**(2), 893–915 (2011)
2. Baeza, A., Mulet, P., Zorío, D.: High order weighted extrapolation for boundary conditions for finite difference methods on complex domains with Cartesian meshes. J. Sci. Comput. **69**(2), 170–200 (2016)
3. Cravero, I., Semplice, M.: On the accuracy of WENO and CWENO reconstructions of third order on nonuniform meshes. J. Sci. Comput. **67**, 1219–1246 (2015)
4. Donat, R., Marquina, A.: Capturing shock reflections: An improved flux formula. J. Comput. Phys. **125**, 42–58 (1996)
5. Harten, A., Engquist, B., Osher, S., Chakravarthy, S.R.: Uniformly high order accurate essentially non-oscillatory schemes, III. J. Comput. Phys. **71**(2), 231–303 (1987)
6. Holoborodko, P.: MPFR C++. http://www.holoborodko.com/pavel/mpfr/
7. Jiang, G.S., Shu, C.W.: Efficient implementation of Weighted ENO schemes. J. Of Comput. Phys. **126**, 202–228 (1996)
8. Levy, D., Puppo, G., Russo, G.: Central WENO schemes for hyperbolic conservation laws. ESAIM: Mathematical Modelling and Numerical Analysis **33**(3), 547–571 (1999)

9. Liu, X-D., Osher, S., Chan, T.: Weighted essentially non-oscillatory schemes. J. Comput. Phys. **115**(1) 200–212 (1994)
10. The GNU MPFR library. http://www.mpfr.org/
11. Shu, C.-W.: Essentially non-oscillatory and weighted essentially non-oscillatory schemes for hyperbolic conservation laws. In Cockburn, B., Johnson, C., Shu, C.-W. and Tadmor, E. (Quarteroni, A., Ed.): Advanced Numerical Approximation of Nonlinear Hyperbolic Equations. Lecture Notes in Mathematics, vol. 1697, Springer-Verlag, Berlin, 325–432 (1998)
12. Shu, C.-W.: High order weighted essentially nonoscillatory schemes for convection dominated problems. SIAM Rev. **51**, 82–126 (2009)
13. Shu, C.-W., Osher, S.: Efficient implementation of essentially non-oscillatory shock-capturing schemes. J. Comput. Phys. **77**, 439–471 (1988)
14. Shu, C.-W., Osher, S.: Efficient implementation of essentially non-oscillatory shock-capturing schemes, II. J. Comput. Phys. **83**(1), 32–78 (1989)
15. Zhang, Y.-T., Shu, C.-W.: ENO and WENO schemes. Chapter 5 in Abgrall, R. and Shu, C.-W. (eds.), Handbook of Numerical Methods for Hyperbolic Problems Basic and Fundamental Issues. Handbook of Numerical Analysis vol. 17, North Holland, 103–122 (2016)